

In Vivo Aberration Correction for Transcutaneous HIFU Therapy Using a Multielement Array

Gilles P. L. Thomas¹, Tatiana D. Khokhlova¹, Oleg A. Sapozhnikov, Yak-Nam Wang, Stephanie I. Totten, and Vera A. Khokhlova¹

Abstract—One of the challenges of transcutaneous high-intensity focused ultrasound (HIFU) therapies, especially ones relying heavily on shock formation, such as boiling histotripsy (BH), is the loss of focusing from aberration induced by the heterogeneities of the body wall. Here, a methodology to execute aberration correction *in vivo* is proposed. A custom BH system consisting of a 1.5-MHz phased array of 256 elements connected to a Verasonics V1 system is used in pulse/echo mode on a porcine model under general anesthesia. Estimation of the time shifts needed to correct for aberration in the liver and kidney is done by maximizing the value of the coherence factor on the acquired backscattered signals. As this process requires multiple pulse/echo sequences on a moving target to converge to a solution, tracking is also implemented to ensure that the same target is used between each iteration. The method was validated by comparing the acoustic power needed to generate a boiling bubble at one target with aberration correction and at another target within a 5-mm radius without aberration correction. Results show that the aberration correction effectively lowers the acoustic power required to reach boiling by up to 45%, confirming that it indeed restored formation of the nonlinear shock front at the focus.

Index Terms—Aberration correction, histotripsy.

I. INTRODUCTION

TRANSCUTANEOUS high-intensity focused ultrasound (HIFU) therapies allow for noninvasive thermal or mechanical ablation of multiple abdominal targets, including tumors in the liver, kidney, and pancreas [1], [2]. On the way

Manuscript received 31 May 2022; accepted 15 August 2022. Date of publication 18 August 2022; date of current version 27 September 2022. This work was supported in part by NIH under Grant R01EB007643, Grant R01GM122859, and Grant R01EB025187; and in part by RSF under Grant 20-12-00145. (Corresponding author: Gilles P. L. Thomas.)

This work involved human subjects or animals in its research. Approval of all ethical and experimental procedures and protocols was granted by the Institutional Animal Care and Use Committee (IACUC) under Approval No. PROTO201600534.

Gilles P. L. Thomas, Yak-Nam Wang, and Stephanie I. Totten are with the Applied Physics Laboratory, Center for Industrial and Medical Ultrasound, University of Washington, Seattle, WA 98105 USA (e-mail: gillespierre.thomas@gmail.com).

Tatiana D. Khokhlova is with the Division of Gastroenterology, School of Medicine, University of Washington, Seattle, WA 98105 USA.

Oleg A. Sapozhnikov and Vera A. Khokhlova are with the Applied Physics Laboratory, Center for Industrial and Medical Ultrasound, University of Washington, Seattle, WA 98105 USA, and also with the Physics Faculty, Moscow State University, Moscow 119991, Russia.

Digital Object Identifier 10.1109/TUFFC.2022.3200309

to the target, the HIFU beam typically propagates through multiple layers of tissue of different thickness and with varying sound speed. Due to the ensuing variation of relative time shifts along the HIFU wavefront, i.e., aberration, the focal waveform is distorted and decreased in amplitude, the focal area is widened and spatially shifted, and the side lobes are enhanced [3], [4], [5], [6], [7]. Perinephric and subcutaneous fat has the lowest sound speed of all soft tissues, and as a consequence, the precision, efficacy, and safety of HIFU thermal treatment of targets, such as kidney [5] and breast [8], are especially affected by aberration. For mechanical HIFU ablation approaches relying heavily on shock formation at the focus, such as boiling histotripsy (BH) [9] and shock-scattering histotripsy [10], aberration is a major challenge that can prevent the formation of shock fronts of sufficient amplitude to generate the boiling bubble or bubble cloud required for the treatment [11].

The use of HIFU multielement arrays may allow for compensation of aberrations by introducing appropriate time delays at different array elements, and several approaches to identify those delays have been proposed [12], [13], [14], [15], [16], [17], [18]. In one method, the phases on HIFU array elements are varied to maximize the acoustic radiation force [12], [13], [14]; however, this method was impractical to implement for arrays with a high number of elements, as it requires the emission of a large number of pulses ($4N$ pulses for an array of N elements) for effective correction. To the best of our knowledge, these methods were also never applied *in vivo*. Alternatively, aberration correction using a cavitation bubble nucleated in tissue at the focus as a reflective target for time reversal was also demonstrated [15], [16], [17]. However, those methods are destructive and also have high-power requirements to the HIFU transducer to achieve necessary *in situ* negative pressures to reliably generate the cavitation bubble at the focus [19], [20].

Recently, we have reported on an aberration correction approach adapted from ultrasound imaging [21] that relies on using the HIFU array in the pulse/echo mode with pulse inversion to detect the second harmonic of signal backscattered from the focus [18]. The algorithm used was a hybrid of two aberration correction methods, namely, the nearest neighbor correlation [22] and the beamsum correlation [23], where the beamsum is obtained by summing the backscatter signal received by each element of the array. The echo signals from

diffuse scatterers received by the array elements were cross correlated between the nearest neighbors or with the beamsum, and the lags corresponding to the maximum correlation were used to estimate the time delays resulting from aberrations. These estimated delays were then subtracted from the array elements, and the correction process was repeated iteratively until a convergence of the delays estimate was reached.

In the *in vitro* and *ex vivo* settings, this approach was found to reliably converge toward an estimation of the time delays required to restore the focus to almost non-aberrated level, hence with the shock necessary to BH treatment, with an average of eight iterations, and with a time of at least 300 ms between each iteration needed for computation. Thus, the approach was shown to be very promising in tissue phantoms and *ex vivo*, but not without challenges that could be foreseen for its application *in vivo*. First, similar to the case of tissue imaging, the algorithm relied on the harmonic backscatter from a group of diffuse random scatterers located within the focal area, and the method would refocus the beam toward the strongest scatterer, which was not necessarily located at the focus [22]. Therefore, the result of the correction contained a beam steering component. While the resulting HIFU focus shift was typically quite small (under 1 mm transversely and 3 mm axially) and could be neglected in most cases, this translated into larger interelement time delays and phase wraps during the correction, complicating the process. Second, the algorithm required acquiring backscatter signals from the same group of scatterers at each iteration to converge, so as to keep the steering component of the correction constant. This appeared problematic for *in vivo* implementation in the presence of respiratory and cardiac tissue motion. Interestingly, in the context of ultrasound imaging, those challenges had led to abandoning aberration correction approaches altogether in favor of tissue harmonic imaging (THI) that worked faster and was easier to implement while providing acceptable improvement in image quality [24].

The objective of this work was to address the aforementioned challenges in the context of HIFU treatment and demonstrate the feasibility of this aberration correction algorithm *in vivo*. First, a method to find an estimate of the HIFU beam steering component and remove it during the aberration correction was developed. Second, a target tracking method was implemented to gate the aberration correction pulses so as to acquire echoes from the same set of scatterers in the presence of cyclic movement *in vivo*. Finally, the performance of the method was tested *in vivo* by transcutaneously targeting porcine liver and kidney with a 256-element HIFU array. The correction quality was evaluated by comparing the transducer acoustic power required to generate a boiling bubble at the HIFU focus by a 10-ms pulse with and without aberration correction.

II. MATERIALS AND METHODS

A. HIFU Apparatus

The HIFU transducer used in this study has been described in detail in previous publications from our group [25], [26]. Briefly, it was a 1.5-MHz, 256-element spiral array made of composite piezoelectric material (Imasonic,

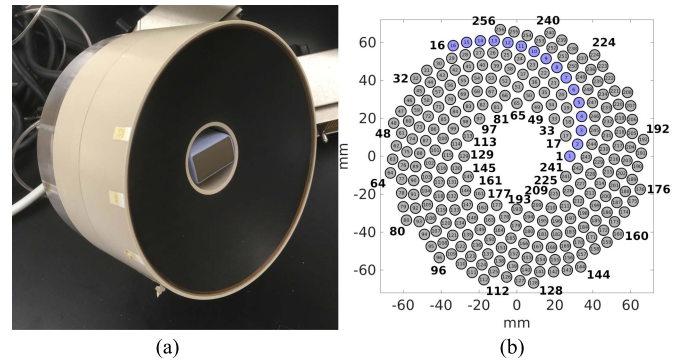


Fig. 1. (a) Photograph of the 256-element HIFU array with its inline imaging probe. (b) Layout of the array elements with one of the 16 spiral arms shown in blue.

Voray-sur-l'Ognon, France) and is shown in Fig. 1. The outer diameter of the array was 144 mm, its nominal focal distance was 120 mm, and a coaxial ultrasound imaging probe (3PE, Humanscan, Gyeonggi-do, South Korea) was inserted in the central opening of 40-mm diameter. The circular elements had a 7-mm diameter and were arranged in 16 spiral branches, each containing 16 elements as shown in Fig. 1(b). This HIFU array could deliver high amplitude shock fronts at the focus, up to 100 MPa in water.

The electrically matched HIFU array was connected to a modified four-board V1 Verasonics (V-1 Ultrasound Acquisition Platform, Verasonics Inc., Kirkland, WA, USA) with HIFU option consisting of the addition of an external 1200-W dc power supply (QPX600DP, Aim-TTI, Huntingdon, U.K.). The modification consisted of seven electrolytic capacitors identical to the internal dc supply capacitor of the system (B41560A9159M000, EPCOS, Munich, Germany) connected in parallel with the external dc power supply, allowing for the sustained delivery of 3.7-kW electric power for a duration of up to 10 ms with a maximum duty cycle of 2%.

The ultrasound phased array imaging probe was connected to a separate two-board V1 Verasonics system and operated in standard B-mode at 4.5 MHz, 128 scan lines at 30 frames/s. The position of the HIFU focus was pre-registered with the system and displayed on the image as a red cross for targeting. The imaging probe was only used for targeting and had no role in the aberration correction algorithm.

B. Signal Acquisition

The signals needed to perform aberration correction were acquired by sending pulse/echo sequences with the HIFU array. A single period of a square electrical input was sent to the array with a central frequency of 1.5 MHz and acoustic power equivalent to a continuous-wave excitation between 68 and 1042 W, depending on the target depth and associated attenuation and aberration of the HIFU beam. At those acoustic power levels, the *in situ* waveform was nonlinearly distorted, facilitating the use of backscattered harmonics to reduce the size of the focal region and, thus, improve the precision and quality of aberration correction, as previously demonstrated [18]. Specifically, the second harmonic was chosen as the signal of interest, and as such, at 68-W acoustic

power, the peak positive pressure at the focus was 12 MPa, the length of the focal region at -6 -dB level was 4.6 mm, and its width at the same level was 0.6 mm in free field in water [18].

To improve the signal-to-noise ratio of the second harmonic of the backscattered signal, a pulse-inversion scheme [27] was used similar to our prior work [18]. Two imaging pulses with the same driving voltage, but opposite polarity (the second pulse was an inverted copy of the first one), were sent and received. The two signals were then directly summed in the buffer of the Verasonics system, resulting in its first and third harmonics canceling out, and its second harmonic doubling in value. The acquired signals were sampled at 45 MHz and filtered using a digital Gaussian filter with a center frequency of 3 MHz and a bandwidth of 1.25 MHz at -6 -dB level. Only the signals arriving from the limited depth range of ± 9 mm from the geometric focus of the array were acquired. Finally, the signal was interpolated using a cubic spline interpolation with a factor 16 that was then used in the aberration correction procedure; these data will be referred to as “received backscattered signals $s_i(t)$ ” or “RF signals” throughout the manuscript.

When a pulse/echo sequence was sent through an aberration medium—such as a body wall—into the scattering target tissue, the received backscattered signals on each element of the array had varying delays between them, as visualized in Fig. 2. To quantitatively estimate the level of aberration of the received signal, we evaluated the coherence factor [28] around the focus of the transducer

$$\text{CF}(t) = \frac{(\sum_i s_i(t))^2}{N \sum_i s_i^2(t)} \quad (1)$$

where $\text{CF}(t)$ is the coherence factor, $s_i(t)$ is the received backscatter signal of the element number i of the HIFU array, $N = 256$ is the number of elements of the array, and t is the time. The coherence factor gave a dimensionless measure of the aberration impact on focusing, and its value was independent of the amplitudes of the RF signals, thus making it reliable as a measure of aberration. The region of interest (ROI) $[T_0, T_1]$ to be used in the aberration correction algorithm was centered around the maximum of coherence factor (CF), with length similar to the length of the imaging pulse sent, here $2 \mu\text{s}$. An example of the CF in the case of propagation through an inhomogeneous medium is shown in Fig. 2. The maximum possible value of the CF is defined by the van Cittert–Zernike theorem [29], which defines the maximum correlation possible between two elements of the array. Here, the HIFU array being spherically focused, a signal originating from the HIFU focus and without aberration would arrive synchronously at all elements of the array. This translates to the maximum value of the coherence factor being equal to 1.

C. Aberration Correction Method

Aberration correction implies estimation of the time shift error on each element of the HIFU array to compensate for it. We previously adapted an aberration correction algorithm originally developed for ultrasound imaging to the same transducer array and tested it *in vitro* [18]. In this algorithm, the 3-D

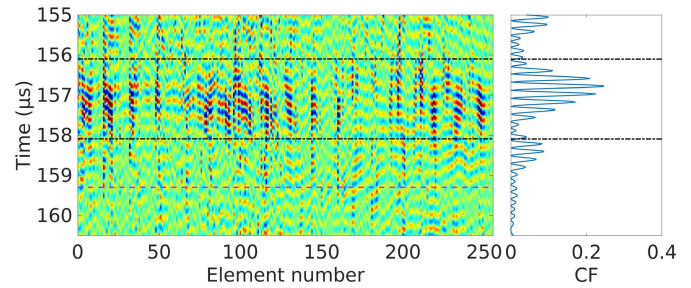


Fig. 2. RF signals $s_i(t)$ of the array elements (vertical colored lines in the left diagram) and their corresponding coherence factor $\text{CF}(t)$ (right plot) acquired from porcine liver *in vivo*. The area between the black dashed-dotted lines corresponds to the ROI for the aberration correction, and the magenta dashed line corresponds to the arrival time of the signals backscattered from the geometric focus of the HIFU array.

transducer array elements were unwrapped into a 1-D path to be able to use nearest neighbor cross correlation. However, the lower quality of the RF signals from *in vivo* conditions resulted in poor cross correlation on certain parts of the unwrapped path, sometimes leading to low correction quality and phase wraps. Therefore, a more reliable algorithm that accounted for the 2-D spatial distribution of the elements was implemented here.

As such, the algorithm for aberration correction used here has been adapted to the HIFU array from an algorithm developed for 2-D ultrasound imaging array by Liu and Waag [30]. Since this aberration correction algorithm relies on cross correlation of the backscatter signals from neighboring elements, it refocuses toward the strongest scatterers [22], which translates into maximizing the beamsum [23].

As the aberration correction algorithm naturally refocused and, thus, steered, toward the strongest scatterer, before compensating for aberrations, we estimated those steering delays and removed them from the RF signals to be used in the aberration correction algorithm. This would bring two benefits: the interelement delays would be lower, reducing greatly the risk of phase wraps during the interelement cross correlations, and also, those estimated steering delays would be removed from the final aberration correction delays, minimizing the impact that aberration correction has on the targeting accuracy [18]. To estimate the (x, y, z) steering component of the scatterer, which was contained within the focal region of the second harmonic, we used an approximation that there were no aberrations; i.e., the scatterers were in a homogeneous medium with a known speed of sound c_0 . We could then, based on the delay-and-sum procedure, determine (x, y, z) by solving the following optimization problem:

$$\begin{aligned} \min_{x,y,z} \Phi(x, y, z) &= - \int_{T_0}^{T_1} \left(\sum_i s_i(t - \tau_i^s(x, y, z)) \right)^2 dt \\ \text{with } \tau_i^s(x, y, z) &= \frac{T_0 + T_1}{2} - \frac{\sqrt{(x_i - x)^2 + (y_i - y)^2 + (z_i - z)^2}}{c_0} \\ \text{s.t. } |x| &\leq x_m, \quad |y| \leq y_m, \quad |z| \leq z_m \end{aligned} \quad (2)$$

where the parameters to be optimized (x, y, z) correspond to the steered position of the HIFU array focus relative to the center of curvature of the transducer [i.e., the array’s

geometric focus position of the array in water without aberrations $(0, 0, 0)$, the values of τ^s are the delays resulting from the steered focus position, the values of (x_i, y_i, z_i) are the coordinates of the center of the i th element of the HIFU array relative to the center of curvature of the transducer, c_0 is the sound speed in water chosen here as 1500 m/s, and T_0 and T_1 are the arrival times corresponding to the start and end of the ROI, respectively. The objective function $\Phi(x, y, z)$ corresponds to the integral over the ROI of the squared beamsum of the RF data accounting for the steering delays introduced. As presented earlier, the ROI was chosen as centered on the area of RF signals presenting the highest value of coherence factor close to the geometric focus position, and its size was set as approximately the length of the pulse sent, which is here about $2 \mu\text{s}$, as shown in Fig. 2. The optimization was also constrained to a space defined here by $x_m = y_m = 1.2 \text{ mm}$ and $z_m = 9 \text{ mm}$, which corresponds to twice the size of the unaberrated focal volume at the second harmonic of the HIFU transducer.

As there were only three parameters to be optimized—the estimated steering component coordinates (x, y, z) —this optimization problem could be solved quickly using various methods. Here, the objective function Φ was derivable with its gradient being

$$\begin{aligned} \frac{\partial \Phi}{\partial x} &= -\frac{2}{c_0} \int_{T_0}^{T_1} \left(\sum_i \frac{x_i - x}{A_i} \frac{\partial s_i}{\partial t}(t) \right) \left(\sum_i s_i(t - \tau_i^s) \right) dt \\ \frac{\partial \Phi}{\partial y} &= -\frac{2}{c_0} \int_{T_0}^{T_1} \left(\sum_i \frac{y_i - y}{A_i} \frac{\partial s_i}{\partial t}(t) \right) \left(\sum_i s_i(t - \tau_i^s) \right) dt \\ \frac{\partial \Phi}{\partial z} &= -\frac{2}{c_0} \int_{T_0}^{T_1} \left(\sum_i \frac{z_i - z}{A_i} \frac{\partial s_i}{\partial t}(t) \right) \left(\sum_i s_i(t - \tau_i^s) \right) dt \quad (3) \end{aligned}$$

where A_i is the distance between the i element of the array and the steered focus, i.e., $A_i = ((x_i - x)^2 + (y_i - y)^2 + (z_i - z)^2)^{1/2}$, and the value of $\partial s_i / \partial t$ was determined numerically using the derivative of the cubic spline interpolation. Thus, a gradient-based optimization algorithm, sequential least square programming (SLSQP) [31], [32] from the NLOpt [33] nonlinear optimization library, was run to find the resulting steering component estimation (x, y, z) . For the first pulse/echo iteration, the initial guess of the parameters to be optimized was set as $x = y = z = 0$. As the same ROI—and thus the same group of scatterers—is targeted at each iteration, the steering position value would vary by less than 5% relative to the previous iteration. Therefore, in subsequent iterations, the value of (x, y, z) of the previous iteration was used as the initial guess for the optimization problem for faster convergence.

Once the optimal parameters (x, y, z) were found, the delays τ^s corresponding to the steering component estimation were removed from the RF signals that the aberration correction algorithm used. The next step of the algorithm was cross correlating of the RF signal of each element with the RF signals from their nearest neighbor elements. Due to the spiral arrangement of the HIFU array, selecting neighboring elements was not as straightforward as in the case of a 2-D grid array originally presented in [30]. Therefore, we chose a radius

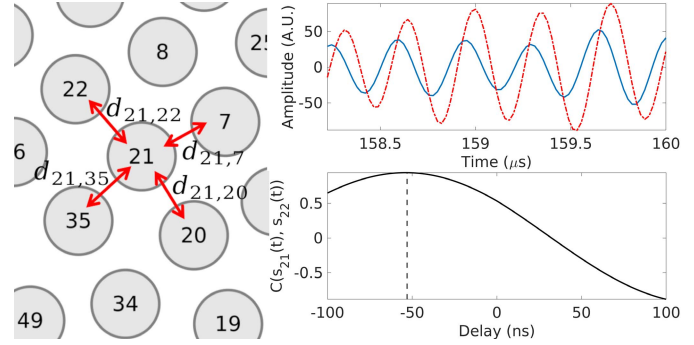


Fig. 3. Illustration of the calculation of the interelement delay d_{ij} for the spiral array. The RF signals on elements 21 and 22 within the ROI are plotted in blue and red, respectively. Their cross-correlation function is plotted in black, with the vertical dashed line corresponding to the value of delay $d_{21,22}$ at the peak of the function.

value r_c as the maximum distance between two center points of elements for them to be considered neighbors. The value of r_c should be as low as possible to have the best signal correlation between the elements, while also including elements in all directions—specifically here, it should include at least one element from the closest spiral branches as well as elements from its own spiral branch. As such, the value was set to $r_c = 8 \text{ mm}$, resulting in most elements having four neighbors—with two neighbors belonging to other spiral branches—and the border elements having at least two neighbors. This led to a total of 448 unique pairs of elements where RF signals were to be cross correlated using the normalized cross-correlation function shown in the following equation:

$$c_{ij}(t) = \frac{\int_{T_0}^{T_1} s_i(\tau) s_j(t + \tau) d\tau}{\sqrt{\int_{T_0}^{T_1} |s_i(\tau)|^2 d\tau \int_{T_0}^{T_1} |s_j(\tau')|^2 d\tau'}} \quad (4)$$

where i and j are the element numbers to be cross correlated. The maximum lag time of the cross-correlation function was chosen as $\pm 100 \text{ ns}$ to avoid phase wraps. The relative delays d_{ij} between backscattered signals on two elements i and j backscattered signals were found as the lag at the peak value of the cross correlation \hat{c}_{ij} , as illustrated in Fig. 3. To avoid errors from poorly correlated signals, the value of d_{ij} was set to 0 for cases where \hat{c}_{ij} was less than 0.7.

Once all the values of d_{ij} were found, the estimate of the correction time delays τ^c to be applied to each element to compensate for aberration could be calculated as $d_{ij} = \tau_i^c - \tau_j^c$ by definition. However, the problem was overdetermined as we had 448 values for d_{ij} and only 256 values possible for τ^c . As such, the following least-mean-square cost function was solved instead to find the best fit:

$$\sum_{i,j} (\tau_i^c - \tau_j^c - d_{ij})^2 \quad \forall \{i, j\} \text{ forming a pair} \quad (5)$$

where the value of the delay of element 1, τ_1^c , was set to 0 as to serve as a reference point. This problem can be easily solved using the ordinary least squares method, as in the original article [30]. Setting the value of τ_1^c arbitrarily did not impact the correction, as it was the relative time delays between the elements, imposed by difference in acoustic propagation path

that impacted the focal waveform. As the Verasonics system required positive time delays input, the following operation was performed to impose $\tau_k^c \geq 0, \forall k \in [1, 256]$:

$$\tau^c = \tau^c - \min(\tau^c). \quad (6)$$

The sum of both the steering and aberration correction delays was then implemented on the HIFU array elements for the next pulse/echo iteration, and this process was repeated until the maximum of the coherence factor reached a plateau—the relevant criterion was a change of less than 2% from the previous iteration. Once the correction converged, the delays τ^c corresponding to the aberration correction were saved to be implemented for the HIFU treatment.

D. Tracking Method

One of the main challenges of applying this aberration correction method *in vivo* was the need to acquire signals from the same set of scatterers at each pulse/echo iteration in the presence of tissue motion. Since the dominating tissue motions—respiratory and cardiac—are quasi-cyclic, it is possible to gate the aberration correction pulses at the same point of every cycle, and this requires a way to track the RF signals pattern within the ROI.

Therefore, a tracking pulse/echo sequence was introduced immediately preceding each aberration correction pulse/echo sequence at every iteration of the aberration correction process. The tracking pulses of the same amplitude as for the aberration correction were emitted by the HIFU transducer elements simultaneously at the fundamental frequency of 1.5 MHz without any time delays, and the backscattered echoes were acquired from the same region as that used in the aberration correction sequence, i.e., ± 9 mm axially around the geometric focus, with no filtering, as opposed to the previously described aberration correction procedure, where a pair of mutually inverted pulses is used with appropriate filtering of nonlinear harmonics by the pulse inversion algorithm. As presented in Fig. 4, following each tracking pulse, the aberration correction imaging pulses were emitted with a time delay of $t_p = 220 \mu\text{s}$ to make sure that the pulses will not interfere with each other, and the whole ensemble of pulses was repeated at a pulse repetition frequency (PRF) of $f_{acq} = 100$ Hz for a total time $T_{acq} = 4$ s, with all the backscattered echoes from all ensembles saved for processing. The repetition period of 0.01 s corresponding to this PRF was short enough, so that the movement of the body from pulse to pulse was negligible. The value of T_{acq} was chosen as slightly longer than the longest period of cyclic motion—the respiratory motion, which is 3–4 s in our case.

The acquired backscattered echoes from the tracking pulse were used as a reference to find the same scatterers at each iteration of the aberration correction process. As cross correlation between the tracking echoes from each of the 256 elements would be computationally costly and slow, the beamsum was used instead:

$$B_n^T(t) = \sum_{i=1}^N S_i(t) \quad (7)$$

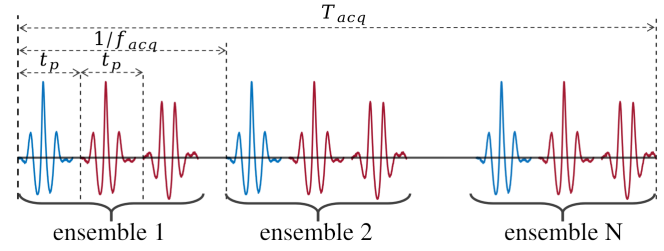


Fig. 4. Acquisition sequence of the tracking (—) and aberration correction with pulse inversion (—) pulses.

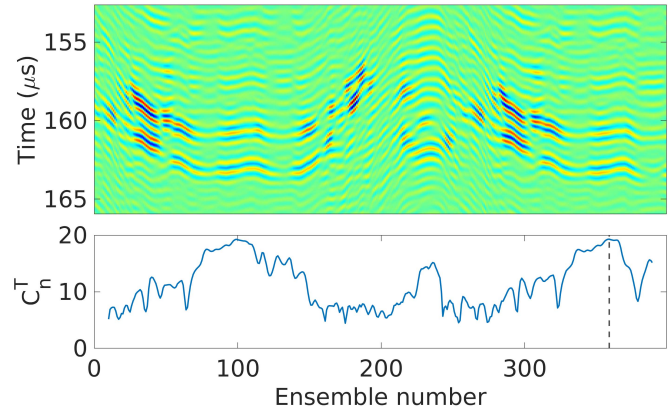


Fig. 5. Top: tracking pulse/echo beamsums $B_n^T(t)$ of each ensemble during one acquisition. Bottom: score C_n^T calculated for each ensemble. The ensemble with the highest score—which tracking beamsum will serve as a reference for future iterations—is highlighted with a vertical dashed line.

where $S_i(t)$ is the unfiltered RF signal of the i th element. For the first aberration correction iteration, a reference tracking signal was set as follows. We chose the set of scatterers that moved the least during the cyclic motion; this was done by cross correlating the tracking beamsum signal within a small lag window of ± 120 ns with beamsums of a number of its preceding and following signals using the following cross correlation function:

$$C_{nm}^B(t) = \frac{\int B_n^T(\tau) B_m^T(t + \tau) d\tau}{\sqrt{\int |B_n^T(\tau)|^2 d\tau \int |B_m^T(\tau')|^2 d\tau'}}. \quad (8)$$

The maxima of all resulting cross correlation functions were then summed to form a score C_n^T

$$C_n^T = \sum_{k=-N_p}^{N_p} \max_{|l| \leq 120 \text{ ns}} (C_{n,n+k}^B); \quad k \neq 0 \quad (9)$$

where n is the ensemble number, and N_p is the number of ensembles to consider for the scoring. Here, we chose $N_p = 10$, resulting in C_n^T reaching a maximum for the group of scatterers that move the least during a 200-ms window, and thus, its RF signals at that maximum were used for the first iteration of the aberration correction algorithm, and its tracking pulse/echo beamsum was saved as a reference $B_{ref}^T(t)$ for the following iterations. This process is illustrated in Fig. 5.

For the remaining of the aberration correction iterations, the tracking pulse/echo beamsums of each ensemble were cross

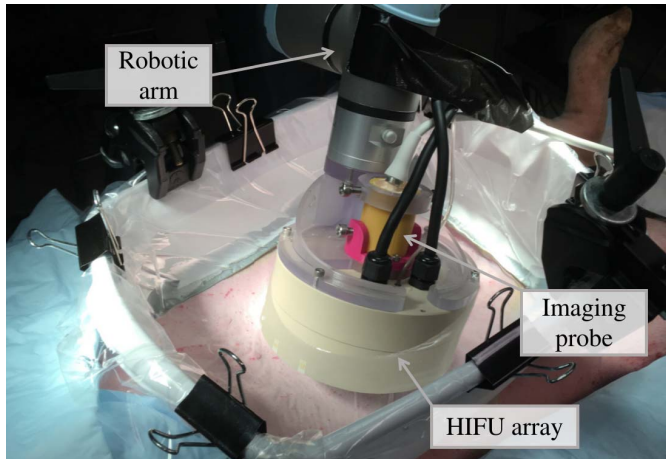


Fig. 6. Photograph of the experimental setup used for the *in vivo* aberration correction.

correlated only with the reference beamsum $B_{\text{ref}}^T(t)$ in (8), i.e., $c_{n,\text{ref}}^B(t)$. The RF signals from the ensemble that yielded the maximum of cross correlation within a ± 120 -ns window for t were used in the aberration correction algorithm for that iteration. If the maximum of the cross correlation $\hat{c}_{n,\text{ref}}^B$ was less than 0.9, a new acquisition was made, and if $\hat{c}_{n,\text{ref}}^B$ was less than 0.9 again, the tracking was considered lost, and the aberration correction process was canceled.

E. Experimental Procedures

Aberration correction *in vivo* was performed when transcutaneously targeting the liver and kidneys of four female domestic swine weighting 43–47.3 kg. All procedures for the animal experiments followed the protocols approved by the Institutional Animal Care and Use Committee at the University of Washington, Seattle, WA, USA. Before the experiment, the animal was pre-medicated with Telazol, then masked with isoflurane, and intubated. Importantly, throughout the experiment, the pigs were free-breathing, not ventilated. When targeting the liver, the pigs were placed on the surgical table in supine position, and when targeting of the kidney—in lateral position. The skin over the targeted organs was shaved, depilated, and cleaned. A thin plastic membrane supported by a solid plastic frame was filled with degassed water and coupled to the animal skin with ultrasound gel. The water was degassed below 10% oxygen saturation using a degassing and filtering system built in-house, and the gel was degassed via centrifugation. The HIFU transducer array and its inline ultrasound imaging were mounted on a robotic arm (UR3e, Universal Robots, Odense, Denmark) using a custom 3-D-printed holder. A photograph of the setup of the experiment during the aberration correction is shown in Fig. 6.

In this study, both the liver and the kidney were targeted subcostally, i.e., in the areas that were unobstructed by the ribs. The thickness of the body wall ranged within 18–29 mm, and the depth of the targeted region ranged within 10–50 mm in the liver and around 10 mm in the kidney cortex. An example of the inline ultrasound image of the targeted area of the liver is shown in Fig. 7.

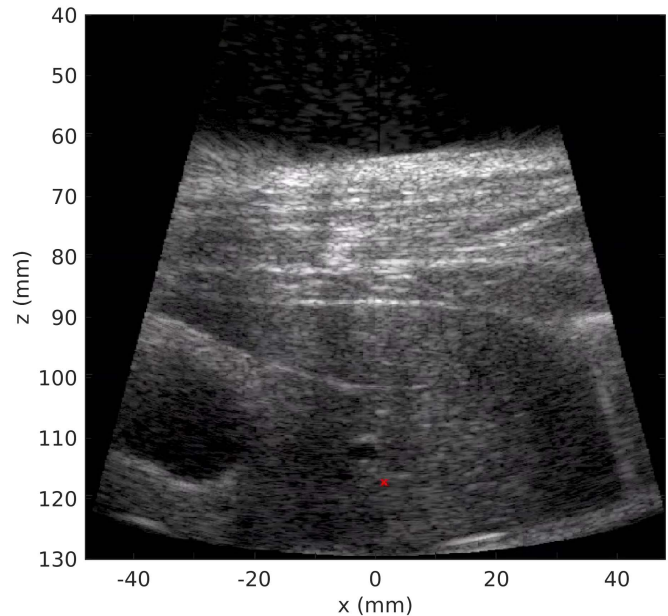


Fig. 7. B-mode ultrasound imaging of the body wall and liver with the inline ultrasound probe of the HIFU transducer. The red cross represents the HIFU geometric focus position.

Throughout the duration of the experiment, the respiration rate ranged within 17–28 breaths/min, and the heartbeat within 90–190 beats/min. Therefore, the longest period of tissue motion was about 3.5 s, which was shorter than the tracking acquisition time $T_{\text{acq}} = 4$ s.

The aberration correction process is illustrated with a diagram in Fig. 8. First, the RF signals were selected within T_{acq} using the tracking algorithm as described in Section II-D, also yielding a tracking reference beamsum B_{ref}^T for the following iterations of correction. The ROI for the aberration correction (the values of T_0 and T_1) was then selected, centered around the scatterers with the highest CF. The aberration correction process described in Section II-C was then launched and ran iteratively until the convergence criterion was reached—difference of maximum of CF being lower than 2% between two iterations. The aberration correction algorithm and the tracking were implemented in MATLAB.

Overall, five areas in the liver and three areas in the kidney were targeted in this study, with at least 20 mm transversely between the areas located in the same organ, to ensure different levels of aberration. Once a target point was identified on inline ultrasound imaging, the aberration correction procedure described earlier was implemented, and the time delays τ^c for aberration correction were determined and applied to all elements of the HIFU array. The quality of correction was evaluated by measuring the HIFU transducer driving voltage sufficient for generating a boiling bubble at the focus with a 10-ms-long pulse, i.e., the threshold of initiation of BH. As this HIFU array was fully characterized previously [25], the voltage threshold was converted to acoustic power when reporting the results. This threshold was then compared with the one without any aberration correction time delays implemented. The rationale for this metric of success is based on the

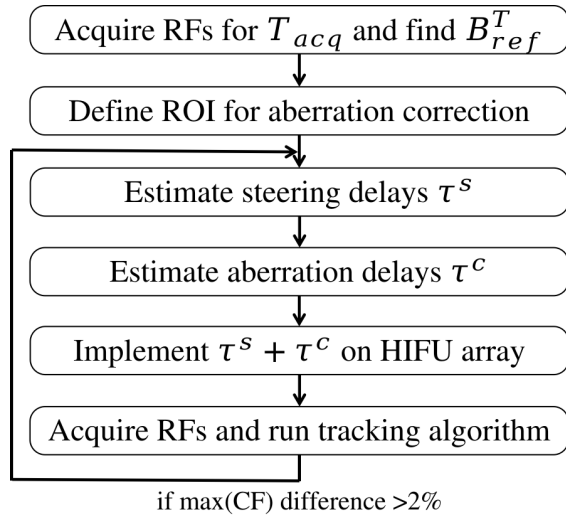


Fig. 8. Flow diagram of the full aberration correction process during the experiments.

boiling threshold being directly linked to the shock amplitude at the focus [34], which the correction procedure was meant to restore [18]. Thus, the boiling threshold was expected to be lower with correction than without it.

In the evaluation procedure, the 10-ms BH pulse was emitted at gradually (in steps of 1 V) increasing HIFU transducer driving voltage starting from 16 V, which corresponded to the minimum voltage needed to generate a boiling bubble with this HIFU transducer in *ex vivo* porcine liver without any aberration. The time between BH pulses was at least 5 s to avoid heat accumulation at the focus. The BH pulses were gated by ultrasound imaging-based tracking of the respiration cycle described in detail in our previous publication [35] to ensure that the targeted region was the same as the one used for aberration correction. Initiation of boiling at the focus was confirmed by visually observing a hyperechoic region of at least 1-mm diameter appearing at the focus [36]. Specifically, one B-mode image was acquired 5 ms before the BH pulse and four B-mode images starting 10 ms after the end of the BH pulse at a framerate of 40 Hz. Those images were then viewed in a different window to facilitate and simplify the detection of the transient hyperechoic region corresponding to the boiling bubble. An example of two of such images is shown in Fig. 9.

Once the BH threshold with aberration correction was found, the transducer was moved by 5 mm in the lateral direction using the robotic arm. This was done to avoid targeting an area that was affected by the previous BH pulses, thus potentially containing bubble nuclei, while keeping the same level of aberration. The aberration correction delays were then removed from the HIFU array elements, and the BH threshold was found using the same procedure.

III. RESULTS

The procedure of aberration correction took between 40 and 80 s and four to nine iterations. The first iteration was always the longest due to the additional time needed to identify the reference beamsum signal for tracking—about 1 s. In the

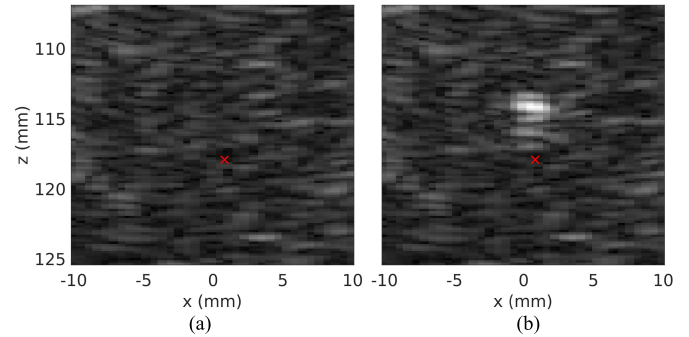


Fig. 9. B-mode imaging around the focus of the HIFU array, where (a) is the image 5 ms before the BH pulse and (b) is the image 10 ms after the pulse. The hyperechoic spot corresponds to a boiling bubble. The red cross represents the HIFU geometric focus position.

following iterations, the time spent on tracking procedures was on the order of 100 ms. Similarly, the time spent on estimating the steering component within the aberration correction process was longer in the first iteration than in the following ones, as the initial value for steered coordinates was set to (0, 0, 0). It was highly variable, depending on the size of the window $[T_0, T_1]$ and the identified steering value, and ranged within 0.1–1 s. As for the following iterations, because the initial guess of the position was set to the previously found value, and that this position was almost constant due to the tracking, the optimization convergence was quick and took less than 100 ms. The remainder of the aberration correction algorithm took between 200 and 400 ms, depending only on the size of the window $[T_0, T_1]$.

The results of the evaluation of aberration correction quality are presented in Table I, and an example of the output of aberration correction iterations is shown in Fig. 10. As seen, the effect of the aberration correction on BH initiation threshold was more noticeable for liver than for kidney and corresponded to 15%–45% decrease in acoustic power. In the case of kidneys, the difference in acoustic power between corrected and uncorrected cases was not as large, within 8% and 21%. This is consistent with prior observations that the level of aberration in porcine body wall overlaying the kidney is much lower than that overlying the liver due to the distribution of the fat layers primarily on the abdomen and not on the sides [11]. This was also reflected in the number of aberration correction iterations needed to converge, on average 5, which is lower than in the liver.

Another observation was that the acoustic power required to reach boiling after aberration correction was consistent for different locations in the liver and the kidney, at around 900 and 660 W, respectively, whereas without correction, it varied more widely. Therefore, an estimation of the theoretical acoustic power required to reach boiling where only the attenuation is accounted for was calculated and added to Table I using the following derating formula [37]:

$$A_{th} = A_0 e^{2(\alpha_{bw} h_{bw} + \alpha_r (h_r - h_0))} \quad (10)$$

where A_{th} is the theoretical acoustic power required to reach boiling only accounting for attenuation, A_0 is the acoustic power to reach boiling in both *ex vivo* porcine liver and kidney

TABLE I
ABERRATION CORRECTION RESULTS

		Liver					Kidney		
Threshold no correction (W)		1113	> 1854*	1762	1261	973	663	780	842
Threshold with correction (W)		842	1186	973	906	842	608	721	663
Theoretical threshold (W)		817	986	893	697	768	592	592	619
Number of iterations		9	8	7	8	7	5	6	4
Steering component	x	0.5	-0.4	0.9	0.8	-0.3	0.2	-0.9	0.4
	y	-0.3	0.2	-0.3	0	-0.2	0.1	0.1	0.4
estimate (mm)	z	-0.7	-0.3	-1	-0.6	-0.9	-1.2	-1.6	-1.3

*The maximum acoustic power of the HIFU system for a 10 ms BH pulse being 1.8 kW, no boiling was obtained in that case.

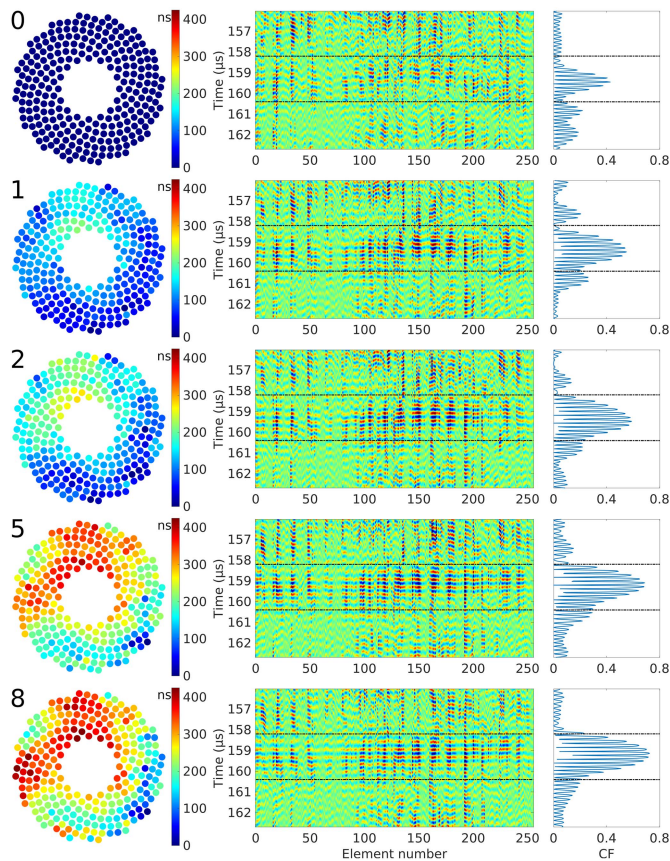


Fig. 10. Example of the evolution of the time delays τ^c (left), RF signals (center), and coherence factor (right) during the iterative aberration correction process in the liver. The iteration number appears on the top-left corner of each step. The area between the black dashed-dotted lines corresponds to the ROI used in the aberration correction algorithm.

tissue at the depth h_0 , $\alpha_{bw} = 1.7$ dB/cm is the attenuation of the body wall [11], α_t is the attenuation of the targeted tissue—here, we only use liver attenuation $\alpha_t = 0.49$ dB/cm [38] as only the liver was targeted at depth other than h_0 , and h_{bw} and h_t are the thickness of the body wall and the depth of the HIFU focus location within the targeted tissue, respectively. Previous *ex vivo* experiments indicated that the acoustic power required to reach boiling in liver and kidney cortex was $A_0 = 288$ W at the depth of $h_0 = 10$ mm [25]. The values of the threshold with correction are close to their estimated theoretical values

only accounting for attenuation, meaning that the aberration correction effectively restored the shock close to non-aberrated level.

The estimated steering component is also given in Table I as an illustration of the extent of the focus displacement if this component was not removed. Its value in the transverse plane (xy) was small and variable, with an average of 0.6 ± 0.26 mm. Its value in the propagation axis (z), however, was mostly dependent on the selection of the window $[T_0, T_1]$ during the correction and had an average of -0.95 ± 0.42 mm.

IV. DISCUSSION AND CONCLUSION

In this article, a method for aberration correction aimed toward *in vivo* transcutaneous HIFU treatment was proposed and tested in a porcine model. Using a multielement HIFU array in tissue harmonic pulse/echo mode on the liver and kidney in an extracorporeal setup, time delays required to compensate for aberration were found. These delays were then applied to the HIFU array elements, and the quality of the correction was evaluated by looking at the acoustic power required to reach boiling at the focus within a 10-ms pulse typical for BH. The acoustic power was reduced by at least 45%—as, in some cases, boiling would not be possible without correction due to the electrical power limitation of the system—compared with the equivalent case without correction, confirming the feasibility and utility of the aberration correction procedure.

An algorithm for retrieving the time shifts due to aberration error on each element of the HIFU array was adapted from a method previously developed for ultrasound B-mode imaging with 2-D arrays. As this algorithm requires multiple iterations of pulse/echo acquisitions of the exact same group of scatterers, and the body is under constant cyclic motion caused mainly by the heartbeat and breathing, a scatterer tracking scheme was introduced. While fairly simple, it proved to be fast and efficient, as no tracking issues were encountered with the exception of cases where the targeted region was moved unexpectedly by motions other than cyclic. A failure of the tracking meant that the scatterers pattern at the focus had changed, which would result in either failure of the aberration correction or an increased number of iterations required to reach convergence. Its main drawback was that it made the overall correction rather long due to the recording time it required—4 s here, chosen as slightly longer than the slowest cyclic motion of the body. While it would seem attractive to implement more complex tracking methods, combined, for example, with active motion compensation with a robotic arm, another issue would arise: the aberrating layer—the body wall in this case—would then be in constant movement relative to the HIFU array; thus at each pulse/echo iteration, the aberration pattern would vary, leading to failed convergence. Introducing breath hold would accelerate the process but will not remove the need for tracking, as the heartbeat motion is non negligible, especially in highly perfused organs, such as the liver and the kidney. In that case, considering a minimum heartbeat rate of 60 beats/min, the value of t_{acq} could be set to 1 s, thus almost dividing the entire correction process time by 4.

A method for estimating and removing the spatial beam steering component of the correction was also proposed and tested. It served multiple purposes. First, as this component could be large due to the topology of the targeted tissue and the spreading of the focus caused by the aberrations, removing it improves the accuracy of the treatment. However, the method only provides an estimation of that component, and therefore, the final aberration correction time delays still contain a steering component, albeit greatly reduced. Theoretically, this could also have been done only once, after the entire aberration correction procedure has taken place, by simply finding the steering position that would minimize the sum of all the correction delays. The main advantage of assessing this component at each iteration was the minimization of the interelement delays, thus avoiding any error and phase wraps caused by cross correlation. In the results presented, the maximum time delays introduced by steering ranged between 30 and 110 ns, more than the cross correlation lag of 100 ns. It is important to note here that this estimate does not include the spatial shift of the focus caused by the aberrative layer itself, as that shift does not result in time delays between the array elements.

The overall time to get the aberration compensating time shifts at one focus position was long—about 1 min. It was observed previously [18] that the coherence factor increased dramatically within the first iterations (usually 2 or 3), while then progressing toward a plateau rather slowly. Depending on the needs of the treatment, and the impact those last iterations have on the refocusing of the array, using a lower requirement of the CF increase (2% here) or even a fixed number of iterations could greatly reduce the procedure time. The other limitation of this study was that the aberration correction was performed for only one HIFU focus location—the geometrical focus of the array, whereas the required correction may be different at the locations corresponding to the electronic focus steering limits used during treatment. This aspect is outside the scope of this work.

In conclusion, this study demonstrated that the proposed aberration correction method is practical and applicable *in vivo* and could be used to improve the precision and safety of *in vivo* transcutaneous HIFU treatments. While, here, it was applied in the context of BH, it could be used for any type of HIFU treatment that uses multielement arrays with transmit–receive capabilities.

REFERENCES

- [1] O. Al-Bataineh, J. Jenne, and P. Huber, “Clinical and future applications of high intensity focused ultrasound in cancer,” *Cancer Treatment Rev.*, vol. 38, no. 5, pp. 346–353, Aug. 2012.
- [2] V. A. Khokhlova *et al.*, “Histotripsy methods in mechanical disintegration of tissue: Towards clinical applications,” *Int. J. Hyperthermia*, vol. 31, no. 2, pp. 145–162, 2015.
- [3] L. M. Hinkelman, T. D. Mast, L. A. Metlay, and R. C. Waag, “The effect of abdominal wall morphology on ultrasonic pulse distortion. Part I. Measurements,” *J. Acoust. Soc. Amer.*, vol. 104, no. 6, pp. 3635–3649, 1998.
- [4] T. D. Mast, L. M. Hinkelman, M. J. Orr, and R. C. Waag, “The effect of abdominal wall morphology on ultrasonic pulse distortion. Part II. Simulations,” *J. Acoust. Soc. Amer.*, vol. 104, no. 6, pp. 3651–3664, Dec. 1998.
- [5] R. Ritchie, J. Collin, C. Coussios, and T. Leslie, “Attenuation and defocusing during high-intensity focused ultrasound therapy through perinephric fat,” *Ultrasound Med. Biol.*, vol. 39, no. 10, pp. 1785–1793, Oct. 2013.
- [6] V. Amin, R. Roberts, T. Long, R. B. Thompson, and T. Ryken, “A study of effects of tissue inhomogeneity on HIFU beam,” in *Proc. AIP Conf.*, vol. 829, no. 1, 2006, pp. 201–205.
- [7] Z. Liu, X. Guo, J. Tu, and D. Zhang, “Variations in temperature distribution and tissue lesion formation induced by tissue inhomogeneity for therapeutic ultrasound,” *Ultrasound Med. Biol.*, vol. 40, no. 8, pp. 1857–1868, Aug. 2014.
- [8] L. M. Hinkelman, D.-L. Liu, R. C. Waag, Q. Zhu, and B. D. Steinberg, “Measurement and correction of ultrasonic pulse distortion produced by the human breast,” *J. Acoust. Soc. Amer.*, vol. 97, no. 3, pp. 1958–1969, 1995.
- [9] T. D. Khokhlova, M. S. Canney, V. A. Khokhlova, O. A. Sapozhnikov, L. A. Crum, and M. R. Bailey, “Controlled tissue emulsification produced by high intensity focused ultrasound shock waves and millisecond boiling,” *J. Acoust. Soc. Amer.*, vol. 130, pp. 3498–3510, May 2011.
- [10] L. D. Maxwell *et al.*, “Cavitation clouds created by shock scattering from bubbles during histotripsy,” *J. Acoust. Soc. Amer.*, vol. 130, no. 4, pp. 1888–1898, Oct. 2011.
- [11] T. D. Khokhlova *et al.*, “Pilot *in vivo* studies on transcutaneous boiling histotripsy in porcine liver and kidney,” *Sci. Rep.*, vol. 9, no. 1, pp. 1–12, Dec. 2019.
- [12] E. Herbert, M. Pernot, G. Montaldo, M. Fink, and M. Tanter, “Energy-based adaptive focusing of waves: Application to noninvasive aberration correction of ultrasonic wavefields,” *IEEE Trans. Ultrason., Ferroelectr., Freq. Control*, vol. 56, no. 11, pp. 2388–2399, Nov. 2009.
- [13] Y. Hertzberg, A. Volovick, Y. Zur, Y. Medan, S. Vitek, and G. Navon, “Ultrasound focusing using magnetic resonance acoustic radiation force imaging: Application to ultrasound transcranial therapy,” *Med. Phys.*, vol. 37, no. 6, pp. 2934–2942, 2010.
- [14] L. Marsac *et al.*, “MR-guided adaptive focusing of therapeutic ultrasound beams in the human head,” *Med. Phys.*, vol. 39, no. 2, pp. 1141–1149, 2012.
- [15] M. Pernot, G. Montaldo, M. Tanter, and M. Fink, “Ultrasonic stars for time-reversal focusing using induced cavitation bubbles,” *Appl. Phys. Lett.*, vol. 88, no. 3, Jan. 2006, Art. no. 034102.
- [16] K. J. Haworth, J. B. Fowlkes, P. L. Carson, and O. D. Kripfgans, “Towards aberration correction of transcranial ultrasound using acoustic droplet vaporization,” *Ultrasound Med. Biol.*, vol. 34, no. 3, pp. 435–445, Mar. 2008.
- [17] J. Gateau, L. Marsac, M. Pernot, J.-F. Aubry, and M. Fink, “Transcranial ultrasonic therapy based on time reversal of acoustically induced cavitation bubble signature,” *IEEE Trans. Biomed. Eng.*, vol. 57, no. 1, pp. 134–144, Sep. 2009.
- [18] G. P. L. Thomas *et al.*, “Phase-aberration correction for HIFU therapy using a multielement array and backscattering of nonlinear pulses,” *IEEE Trans. Ultrason., Ferroelectr., Freq. Control*, vol. 68, no. 4, pp. 1040–1050, Apr. 2021.
- [19] J. Gateau, J. Aubry, D. Chauvet, A. Boch, M. Fink, and M. Tanter, “*In vivo* bubble nucleation probability in sheep brain tissue,” *Phys. Med. Biol.*, vol. 56, no. 22, p. 7001, 2011.
- [20] A. D. Maxwell, C. A. Cain, T. L. Hall, J. B. Fowlkes, and Z. Xu, “Probability of cavitation for single ultrasound pulses applied to tissues and tissue-mimicking materials,” *Ultrasound Med. Biol.*, vol. 39, no. 3, pp. 449–465, Mar. 2013.
- [21] S. Krishnan, K. W. Rigby, and M. O’Donnell, “Improved estimation of phase aberration profiles,” *IEEE Trans. Ultrason., Ferroelectr., Freq. Control*, vol. 44, no. 3, pp. 701–713, May 1997.
- [22] M. O’Donnell and S. W. Flax, “Phase-aberration correction using signals from point reflectors and diffuse scatterers: Measurements,” *IEEE Trans. Ultrason., Ferroelectr., Freq. Control*, vol. 35, no. 6, pp. 768–774, Nov. 1988.
- [23] D. L. Liu and R. C. Waag, “Correction of ultrasonic wavefront distortion using backpropagation and a reference waveform method for time-shift compensation,” *J. Acoust. Soc. Amer.*, vol. 96, no. 2, pp. 649–660, 1994.
- [24] F. Tranquart, N. Grenier, V. Eder, and L. Pourcelot, “Clinical use of ultrasound tissue harmonic imaging,” *Ultrasound Med. Biol.*, vol. 25, no. 6, pp. 889–894, 1999.
- [25] C. R. Bawiec *et al.*, “A prototype therapy system for boiling histotripsy in abdominal targets based on a 256-element spiral array,” *IEEE Trans. Ultrason., Ferroelectr., Freq. Control*, vol. 68, no. 5, pp. 1496–1510, May 2020.

- [26] V. A. Khokhlova *et al.*, "Design of HIFU transducers to generate specific nonlinear ultrasound fields," *Phys. Proc.*, vol. 87, pp. 132–138, Dec. 2016.
- [27] P. Jiang, Z. Mao, and J. C. Lazenby, "A new tissue harmonic imaging scheme with better fundamental frequency cancellation and higher signal-to-noise ratio," in *Proc. IEEE Ultrason. Symp.*, vol. 2, Oct. 1998, pp. 1589–1594.
- [28] K. W. Hollman, K. W. Rigby, and M. O'Donnell, "Coherence factor of speckle from a multi-row probe," in *Proc. IEEE Ultrason. Symp.*, vol. 2, Oct. 1999, pp. 1257–1260.
- [29] R. Mallart and M. Fink, "The van Cittert–Zernike theorem in pulse echo measurements," *J. Acoust. Soc. Amer.*, vol. 90, no. 5, pp. 2718–2727, 1991.
- [30] D. L. Liu and R. C. Waag, "Time-shift compensation of ultrasonic pulse focus degradation using least-mean-square error estimates of arrival time," *J. Acoust. Soc. Amer.*, vol. 95, no. 1, pp. 542–555, 1994.
- [31] D. Kraft *et al.*, "A software package for sequential quadratic programming," Institut für Dynamik der Flugsysteme, Oberpfaffenhofen, Germany, Tech. Rep. DFVLR-FB 88-28, 1988.
- [32] D. Kraft, "Algorithm 733: TOMP–Fortran modules for optimal control calculations," *ACM Trans. Math. Softw.*, vol. 20, no. 3, pp. 262–281, Sep. 1994.
- [33] G. S. Johnson *The NLOpt Nonlinear-Optimization Package*. Accessed: Dec. 10, 2021. [Online]. Available: <http://github.com/stevengj/nlopt>
- [34] M. S. Canney, V. A. Khokhlova, O. V. Bessonova, M. R. Bailey, and L. A. Crum, "Shock-induced heating and millisecond boiling in gels and tissue due to high intensity focused ultrasound," *Ultrasound Med. Biol.*, vol. 36, no. 2, pp. 250–267, Feb. 2010.
- [35] G. P. L. Thomas, T. D. Khokhlova, and V. A. Khokhlova, "Partial respiratory motion compensation for abdominal extracorporeal boiling histotripsy treatments with a robotic arm," *IEEE Trans. Ultrason., Ferroelectr., Freq. Control*, vol. 68, no. 9, pp. 2861–2870, Sep. 2021.
- [36] T. D. Khokhlova *et al.*, "Ultrasound-guided tissue fractionation by high intensity focused ultrasound in an *in vivo* porcine liver model," *Proc. Nat. Acad. Sci. USA*, vol. 111, no. 22, pp. 8161–8166, Jun. 2014.
- [37] O. V. Bessonova, V. A. Khokhlova, M. S. Canney, M. R. Bailey, and L. A. Crum, "A derating method for therapeutic applications of high intensity focused ultrasound," *Acoust. Phys.*, vol. 56, no. 3, pp. 354–363, May 2010.
- [38] V. Zderic, A. Keshavarzi, M. A. Andrew, S. Vaezy, and R. W. Martin, "Attenuation of porcine tissues *in vivo* after high-intensity ultrasound treatment," *Ultrasound Med. Biol.*, vol. 30, no. 1, pp. 61–66, Jan. 2004.



Gilles P. L. Thomas received the Engineering degree in general engineering from the École Centrale de Nantes, Nantes, France, in 2014, the Engineering degree in mechatronics engineering and the M.S. degree in control and automation engineering from the Polytechnic School, University of São Paulo, São Paulo, Brazil, in 2014 and 2015, respectively, and the Ph.D. degree in biomedical engineering from the Université Lyon 1, Lyon, France, in 2019.

He is currently with the Applied Physics Laboratory, University of Washington, Seattle, WA, USA, for postdoctoral training.



Tatiana D. Khokhlova received the Ph.D. degree in physics from Moscow State University (MSU), Moscow, Russia, in 2008.

She was with the Applied Physics Laboratory, University of Washington (UW), Seattle, WA, USA, for postdoctoral training, and then completed a research fellowship with the Department of Medicine, UW, where she is currently a Research Assistant Professor. Her research interests include physical acoustics, therapeutic ultrasound, and photoacoustic imaging.



Oleg A. Sapozhnikov received the M.S. degree in physics and the Ph.D. and D.Sc. degrees in acoustics from Moscow State University (MSU), Moscow, Russia, in 1985, 1988, and 2008, respectively.

Since 1996, he has been with the Applied Physics Laboratory, Center for Industrial and Medical Ultrasound, University of Washington, Seattle, WA, USA. He is currently a Professor with the Department of Acoustics, Physics Faculty, MSU. His research interests include physical acoustics, nonlinear wave phenomena, medical ultrasound, including shock wave lithotripsy, high intensity focused ultrasound, and ultrasound-based imaging.



Yak-Nam Wang received the Ph.D. degree in biomedical engineering from the Queen Mary and Westfield College, University of London, London, U.K., in 2000.

She was with the Department of Bioengineering, University of Washington (UW), Seattle, WA, USA, for postdoctoral training. She is currently a Principal Scientist with the Applied Physics Laboratory, UW, where she is involved in performing preclinical ultrasound research.



Stephanie I. Totten received the Associate of Applied Science degree in veterinary technology from the Nebraska College of Technical Agriculture (NCTA), Curtis, Nebraska, in 2013, and the bachelor's degree in veterinary technology from the University of Nebraska-Lincoln (UNL), Lincoln, Nebraska, in 2014.

She was an Assistant Laboratory Animal Technician (ALAT) with the American Association for Laboratory Animal Science (AALAS), Memphis, TN, USA, in 2017. In 2018, she moved to the Department of Medicine-Gastroenterology, University of Washington (UW), Seattle, WA, USA, as a Laboratory Technician. She has been with the Applied Physics Laboratory (APL), Center for Industrial and Medical Ultrasound (CIMU), as the Lead Animal Manager.



Vera A. Khokhlova received the M.S. degree in physics and the Ph.D. and D.Sc. degrees in acoustics from Moscow State University (MSU), Moscow, Russia, in 1986, 1991, and 2012, respectively.

She was appointed by MSU, where she is currently an Associate Professor with the Department of Acoustics, Physics Faculty. Since 1995, she has been with the Applied Physics Laboratory (APL), Center for Industrial and Medical Ultrasound, University of Washington, Seattle, WA, USA. Her research interests include the field of nonlinear acoustics, therapeutic ultrasound, including metrology and bioeffects of high-intensity focused ultrasound fields, shock wave focusing, nonlinear wave propagation in inhomogeneous media, and nonlinear modeling.